Saudi Journal of Biological Sciences 30 (2023) 103520

HOSTED BY

Contents lists available at ScienceDirect

Saudi Journal of Biological Sciences

journal homepage: www.sciencedirect.com

Original article

Functional consequences of Genetics variant in *TMC1* and *TMC2* within a United Arab Emirates family with Pre-lingual hearing loss

Abdullah Al Mutery [a,c,d,*], Walaa Kamal Eldin Mohamed [a,b], Mona Mahfood [a], Jihen Chouchen [d], Abdelaziz Tlili [a,c,d]

[a] Department of Applied Biology, College of Sciences, University of Sharjah, Sharjah, United Arab Emirates
[b] Department de Genètica i de Microbiologia, Facultat de Biociències, Universitat Autònoma de Barcelona, Barcelona, Spain
[c] Human Genetics & Stem Cells Research Group, Research Institute of Sciences & Engineering, University of Sharjah, Sharjah, United Arab Emirates
[d] Molecular Genetics and Stem Cell Research Laboratory, University of Sharjah, Sharjah, United Arab Emirates

ARTICLE INFO

Article history:
Received 7 July 2022
Revised 30 October 2022
Accepted 25 November 2022
Available online 1 December 2022

Keywords:
Non-syndromic Hearing Loss
Whole-exome sequencing
TMC1
c.596A > T mutation
Phenotypic variability
Protein docking

ABSTRACT

Hearing loss (HL) is the most prevalent sensory disorder whose etiology comes from environmental and/or genetic factors. Approximately 60 % of HL cases are due to mutations in genes responsible for maintaining a normal hearing function. Despite the monogenic inheritance of hereditary hearing loss (HHL), its diagnosis is challenging as both clinical and genetic heterogeneity characterizes it. Through the development of next-generation sequencing (NGS) techniques, the number of identified mutations responsible for HHL has increased exponentially during the last decade. Mutations in the *TMC1* have been reported in several patients with nonsyndromic hereditary hearing loss (NSHHL), more precisely in cases with an autosomal recessive inheritance pattern. In this study, we conducted whole-exome sequencing (WES) analysis of a United Arabs Emirates (UAE) family with autosomal recessive nonsyndromic hearing loss (ARNSHL). This analysis revealed segregation of the *TMC1* missense mutation c.596A > T (p.Asn199Ile) with the disease. Bioinformatics analysis supported the pathogenic effect of this mutation and predicted its impact at the proteomics level. Molecular docking analysis of *TMC2*WT, *TMC2*R123K, *TMC2*Q205R, and *TMC2*R123K + Q205R. Finally, protein docking results suggest a role for *TMC2* variants in the phenotypic variability observed within the investigated family.

1. Introduction

Hereditary hearing loss (HHL) is among the most common sensory disorders and is categorized by heterogeneity on multiple levels - clinical, genetic, and allelic (https://hereditaryhear- ingloss.org/). Almost every probable inheritance mechanism for this disease has been described, with prevailing recessive forms (World Health Organization Global Health Estimates, 2016). Around 70 % of all HHL cases are asymptomatic and are classified as non HHL (World Health Organization Global Health Estimates, 2016). Autosomal recessive nonsyndromic HHL (ARNSHHL) represents the glob- ally predominant form of deafness, with 76 genes and 108 loci reported so far (https://hereditary- hearingloss.org/) leading to this condition. Such genetic heterogeneity associated with extreme allelic heterogeneity renders next-generation sequencing (NGS) techniques a sensible approach to unraveling genetic defects related to deafness in patients with HHL. Moreover, this approach can rapidly detect tens of thousands of DNA variants quickly and cost-effectively compared to Sanger sequencing (Giese et al., 2017).

TMC1 (Transmembrane channel-like gene 1) gene mutations were identified as causative for ARNSHL, linked to the *DFNB11 and DFNB7* loci (Global Costs, 2021). *TMC1* gene is the sixth most frequent cause of hereditary hearing loss among all

Abbreviations: **HL**, **Hearing Loss**; **HHL**, **Hereditary Hearing Loss**; **NGS**, **Next Generation Sequencing**; **NSHHL**, **Nonsyndromic Hereditary Hearing Loss**; **WES**, **Whole-Exome Sequencing**; **UAE**, **United Arabs Emirates**; **ARNSHL**, **Autosomal Recessive Nonsyndromic Hearing Loss**; GATK, **Genome Analysis Toolkit**; **GnomAD**, **Genome Aggregation Database**; **PCR**, **Polymerase Chain Reaction**.

* Corresponding author at: Department of Applied Biology, College of Sciences, University of Sharjah, Sharjah, United Arab Emirates.
E-mail addresses: aalmutery@sharjah.ac.ae (A. Al Mutery), Walaa.mohamed@nanoporetech.com (W. Kamal Eldin Mohamed), atlili@sharjah.ac.ae, Abdelaziz.Tlili@fss.rnu.tn (A. Tlili).

Peer review under responsibility of King Saud University.

Production and hosting by Elsevier

https://doi.org/10.1016/j.sjbs.2022.103520
1319-562X/

ARNSHHL-related genes. It accounts for 6 % of deafness cases within Eastern Turkish populations and 3 % to 5 % in European, Tunisian, Pakistani, and Indian communities, respectively (Mehl and Thomson, 2002; Kitajiri et al., 2007; Kalay et al., 2005; Schrauwen et al., 2013). The *TMC1* gene belongs to the gene family predicted for encoding transmembrane proteins (Tlili et al., 2008). It encodes for the transmembrane channel-like protein 1 (*TMC1*), containing six transmembrane domains and one conserved *TMC* domain (Kurima et al., 2002). *TMC1* protein is expressed in the murine organ of Corti and has a significant role in the maturation and survival of inner ear hair follicular cells (Jia et al., 2020). The transformation of a mechanical stimulus to an electrical signal within the cochlea is referred to as mecha-no-electrical transduction (MET) (Kawashima et al., 2011). Evidence suggests that the MET within the inner ear is present as a complex of six differing proteins: *TMC1, TMC2,* TMIE, Protocadherin-15 (PCDH15), Lipoma HMGIC fusion partner-like 5 (LHFPL5), and Calcium and integrin-binding protein 2 (CIB2) (Hudspeth, 1989). Moreover, other gene mutations including mutations in the GJB2 (gap junction protein beta 2) gene are very common and the most prevalent in individuals with hereditary hearing loss (reference). GJB2 mutations are responsible for almost 50 % of all cases with ARNSHL in most populations. This genetic heterogeneity is also emphasized by the variation in frequency of specific mutations among different populations. To date, >100 deafness mutations have been reported in the GJB2 gene (The Connexin-deafness Homepage: https://davinci.crg.es/deafness/).

This study conducted an NGS-based analysis on a United Arab Emirates (UAE) family with hearing loss and negative for *GJB2* mutations. We identified one known-*TMC1* mutation (**c.596**.

A > T) that segregated the disease within the affected family. Bioinformatics and 3D protein modeling analysis confirmed the pathogenic effects of the c.596 A > T mutation on the protein. Moreover, the analysis of variants associated with *MET* genes within all affected individuals suggested a role for *TMC2* variants in the phenotypic variability observed in the studied family.

2. Materials and methods

2.1. Patients and samples

A UAE family affected with ARNSHHL and negative for *GJB2* mutations volunteered to be part of this study regarding their condition. Following audiological and medical evaluations, all patients (or their parents) provided written informed consent. The University of Sharjah's experimental procedures were approved by the Ethics Committee (Sharjah, UAE). Saliva samples were collected using Oragene-DNA® (OG-500) Kit [DNA Genotek™, Canada], and the genomic DNA extraction was performed using the prep IT-L2P® (DNA Genotek™, Canada) protocol.

2.2. Whole exome sequencing and Bioinformatics analysis

The Whole Exome Sequence (WES) was conducted on the probands from each family. DNA was extracted from Saliva using the Oragene-DNA® (OG-500) extraction Kit [DNA Genotek™, Canada]. SureSelect V5-post kit® was employed for capturing genome libraries [Agilent Technologies™, Santa Clara, CA, USA]. Target regions were sequenced at a depth of 142X using 150 bp paired end reads on an Illumina HiSeq 4000® [Illumina™, San Diego, CA, USA]. Burrows- Wheeler Alignment (BWA) (Langmead et al., 2009)tool was used to align sequences to the hu- man reference genome (hg19). The variant call was conducted with the Genome Analysis Toolkit (GATK v4.2.2.0) (McKenna et al., 2010). Annotation of the variants was performed with SnpEff.

v4.1. Variant filtering was conducted as follows: (1) prioritization of variants in candidate genes known to be responsible for hearing loss (2) inclusion of non-synonymous, frameshift, and stop/start codon gains/loss variants; (3) inclusion of variants with < 1 % allele frequency within the Genome Aggregation Database (GnomAD v2.1.1) (https://gnomad.broadinstitute.org); and (4) prediction variant pathogenicity by applying PolyPhen2 and SIFT scores. Sanger sequencing analysis was also performed to validate candidate variants among probands and their segregation within families.

2.3. TMC1 exon 11 amplification

To amplify exon 11 harboring the c.596 A > T mutation, the following primers were used:

*TMC1*_Ex11_F GAAGGCAACCAAGACAAAGC and *TMC1*_Ex11_R ACCCCCTTTAGTG-CAAGGAT. The reaction mixture was prepared using the AmpliTaq Gold™ 360 Master Mix® [NY, USA], and the PCR conditions were 95 °C for 5 min, followed by 35 cycles of 95 °C for 15 s, 53 °C for 30 s, 72 °C for 1 min, concluding with a single extension step at 72 °C for 10 min. The PCR product was size validated using 2 % agarose gel, and the band size was noted to be 376 bp. Prior to the Sanger sequencing reaction, PCR products were treated using the ExoSapIT cleanup® reagent kit [Affymetrix™, USA].

2.4. Sanger sequencing

Big Dye Terminator v3.1 Cycle Sequencing Kit® [Applied Biosystems, Thermo Fisher Scientific TM, USA] was used to sequence the treated PCR products. As a result, the resulting sequencing reactions were purified using the Qiagen TM DyeEX 2.0 spin kit®. Capillary sequencing was carried out on a Genetic Analyzer 3500® platform [Applied Biosystems, Thermo Fisher Scientific TM, USA], and data analysis was performed using the Sequencing analysis software with KB™ SeqScape® Software and Gene mapper software v5.0. Sequenced samples were compared using BLAST with the NCBI Reference Sequence: NG_008213.1.

2.5. In silico analysis of the c.596 A > T mutation

Function of the new variant *c.596 A > T* was predicted and explored by SIFT [https://sift.bii.a- star.edu.sg/], PROVEAN (https://provean.jcvi.org/index.php), and PolyPhen-2 (https://genet- ics.bwh.harvard.edu/pph2/).

2.6. Computational methodologies for predicting mutation impact

The three-dimensional structure of mouse *TMC1* was published by Ballesteros et al., reference. But we haven't utilized this structure as our subject of study was human samples. For this purpose, the wild-type protein sequence of human *TMC1* was retrieved from Uniprot. Consequently, protein homologs to *TMC1* in 9 vertebrates (chimpanzee, rhesus monkey, equine, ca- nine, bovine, murine, brown rat, zebrafish, and chicken) were extracted from Uniprot and Ensembl databases. These sequences were aligned utilizing Clustal Omega using default parameters (https://www.ebi.ac.uk/Tools/msa/clustalo/).

Swiss model (https://swissmodel.expasy.org/interactive) was employed for model building. Web-based modeling was performed for acquisition of comparatively most optimal and reliable model. The web servers including I-TASSER, Phyre2, Robetta, were utilized for prediction of 3D structures for *TMC1 and TMC2.* Furthermore, the predicted 3D models were evaluated by Molprobity and UCLA (https://saves.mbi.ucla.edu/).

Consequently, wild type (w +) and Asn199Ile-mutated (m) isoforms of human *TMC1* were submitted to the Swiss model (https://swissmodel.expasy.org/interactive) for automated structure prediction. Furthermore, possible homology-modeling templates were manually searched in Protein Data Bank (PDB), employing NCBI BlastP. The structures of *TMC1*w + and *TMC1*m were also modeled in Phyre2 and Robetta servers. The Phyre2 and Robetta server's models were further evaluated through the Molprobity online suite. The comparison of the *TMC1* structure published by Ballesteros et al., and the *TMC1* structure predicted in this study was also made using UCLA structure validation server (https://saves.mbi.ucla.edu/) to avoid any constraints.

Due to the absence of the experimentally established structure of human *TMC2*WT, I- TASSER (World Health Organization Global Health Estimates, 2016) was utilized to predict the 3D structure. The model with reasonable values of C-.

scores were selected. Furthermore, to explore the effect of mutated *TMC2* on *TMC1-TMC2* binding, the 3D structure of *TMC2*R123K, *TMC2*Q205R and *TMC2*R123K + Q205R were predicted using the *TMC2*WT structure as a template via MODELLER 10.1 tool (Giese et al., 2017). Verifications of the predicted models were carried out by the MolProbity tool (Global Costs, 2021). 's Structure refinement and optimization was carried out by the Yasar server (Pacentine and Nicolson, 2019).

Molecular docking analysis of *TMC*2WT, *TMC2*R123K, *TMC2*Q205R, and *TMC2*R123K + Q205R against *TMC1*N199I was accomplished by PatchDock (Gorlin et al., 1995), along with the refinement and re-scoring tool FireDock (Diaz-Horta et al., 2012); to identify the binding domain of *TMC2* responsible for interacting with *TMC1*. In PatchDock, the input parameters were the PDB coordinate files of *TMC1* and *TMC2*. Each candidate transformation was evaluated using a scoring function that was geometrically consistent with the atomic desolvation energy (Jain et al., 1995). Finally, Root Mean Square Deviation (RMSD) was used to eliminate redundant solutions from the candidate solutions. To analyze their conformational alterations, the best-docked structures of the top-ranked solutions were chosen and visualized using UCSF Chimera 1.11.2. (Tlili et al., 2008).

3. Results

3.1. Clinical description: Hearing loss is an autosomal recessive trait

A large UAE consanguineous family was investigated, including three patients with congenital deafness. The pedigree analysis suggested an autosomal recessive inheritance pattern (Fig. 1). Audiogram analysis (Fig. 1) revealed profound deafness in one affected individual and severe-to-profound deafness in the two other affected siblings. Interestingly, all affected siblings had undergone cochlear implantation in their right ears, and their hearing exhibited improvement at low frequencies (250 and 500 Hz).

3.2. Clinical description: Hearing loss is an autosomal recessive trait

A large UAE consanguineous family was investigated, including three patients with congenital deafness. The pedigree analysis suggested an autosomal recessive inheritance pattern (Fig. 1). Audiogram analysis (Fig. 1) revealed profound deafness in one affected individual (II-3) and severe-to-profound deafness in the two other affected siblings (II-2 and II-5). Interestingly, all affected siblings had undergone cochlear implantation in their right ears, and their hearing exhibited improvement at low frequencies (250 and 500 Hz).

3.3. Molecular analysis: Hearing loss trait is linked to c.596A > T mutation in TMC1

The *GJB2* gene was screened for mutations to identify the disease-causing mutation within the investigated family, but no pathogenic variants were identified. Consequently, WES has performed in II-2 and II-3 affected individuals, generating 129,497 and 136,072 variants, respectively. After considering only homozygous variants with a frequency < 0.001, these numbers were reduced to 6,881 and 7,587, respectively. After screening rare DNA variants between these affected individuals, and the ones located within genes responsible for ARNSHHL, we obtained a total of 19 variants (Table 1). Eighteen DNA variants were located within

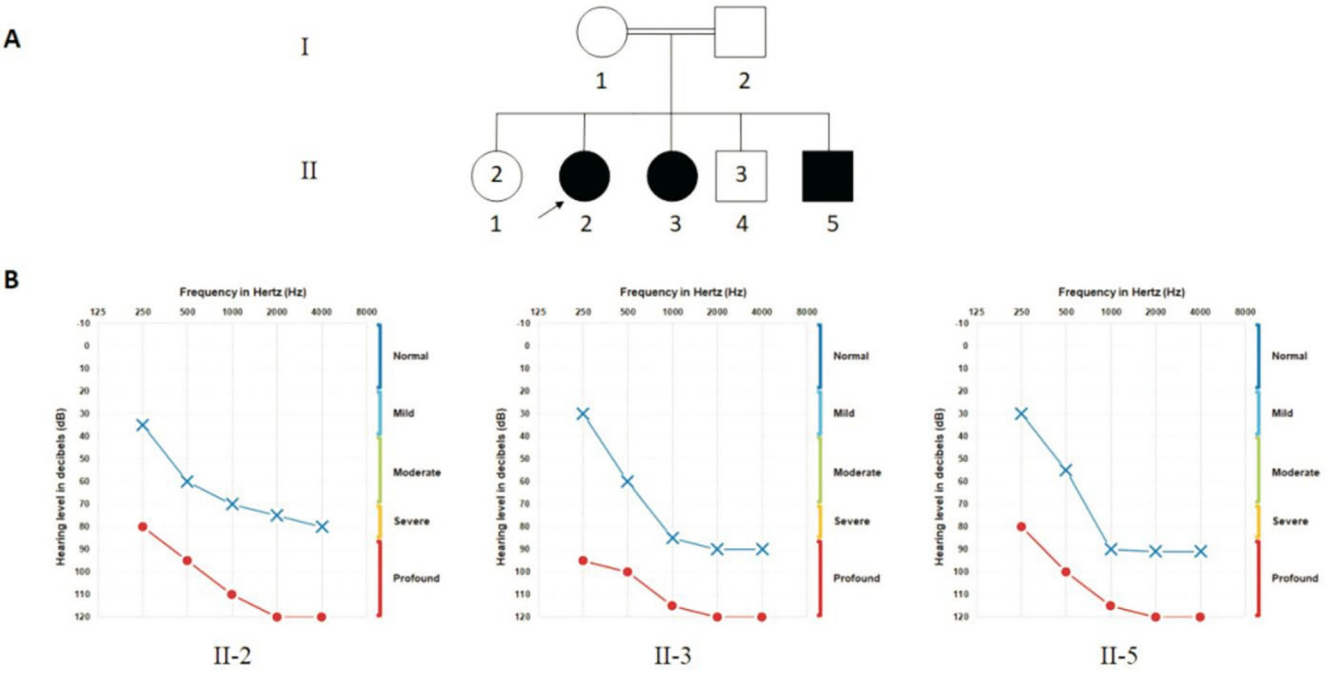

Fig. 1. (A) Pedigree of the family analyzed in this study. (B): Audiogram of the affected individuals.

Table 1
Cross analysis **results.** Rare variants between samples II-2 and II-3 are located within ARNSHHL genes.

Chromosome	Gene	DNA variation	Location	Consequence
6	*COL11A2*	c.3594 + 56dupG	Intronic	–
7	*HGF*	c.865 + 6443_865 + 6442insGTGTGTGT GTGTGTGT	Intronic	–
7	*MET*	c.2638-23del	Intronic	–
8	*ESRP1*	c.644 + 52dupT	Intronic	–
9	*TMC1*	c.596 A > T	Exonic	Missense
9	*TMC1*	c.1695 + 36delT	Intronic	–
11	*EPS8L2*	c.1753 + 8G > C	Intronic	–
11	*MYO7A*	c.2587-110_2587-111in-sCTGCCAAATTATTTGG	Intronic	–
11	*MYO7A*	c.3108 + 81dupG	Intronic	–
11	*MYO7A*	c.3285 + 91dupA	Intronic	–
11	*MYO7A*	c.3751-118_3751-119insGCTGGGGCCTGGAGC	Intronic	–
12	*OTOGL*	c.1133-115dupT	Intronic	–
12	*OTOGL*	c.1684 + 60_1684 + 63dup	Intronic	–
12	*OTOGL*	c.2439-44delA	Intronic	–
12	*OTOGL*	c.6094 + 48dupT	Intronic	–
12	*PTPRQ*	c.1175–38 T > A	Intronic	–
12	*PTPRQ*	c.1870 + 33_1870 + 35	Intronic	–
15	*CIB2*	c.198 + 503 T > C	Intronic	–
17	*MYO15A*	c.6957-64A > G	Intronic	–

intronic regions, and only one was within a coding region, located on *TMC1* and representing a missense mutation: c.596 A > T (p. Asn199Ile).

3.4. Missense mutation c.596 A > T led to Drastic structural changes in TMC1

The protein sequences of human (Uniprot ID: Q8TDI8) and murine (Uniprot ID: Q8R4P5) *TMC1* were aligned with homologs of chimpanzee, rhesus monkey, equine, canine, bovine, brown rat, zebrafish, and chicken (Ensembl identifiers: XP_016816447.1, XP_014973432.1, XP_023482822.1, XP_022283106.1, XP_024851786.1, NP_001101991.1, XP_021331962.1, and NP_001006580.1, respectively) using Clustal Omega. The Asn199 change in human *TMC1* was conserved across all lineages. SIFT, PolyPhen, and PROVEAN analyses demonstrated that this mutation is considered harmful, probably damaging, and deleterious, respectively.

The impact of the missense mutation within the *TMC1* protein structure was predicted using multiple databases and software packages. The Swiss model (https://swissmodel.expasy.org/interactive) yielded four *TMC1*$^{w+}$ and *TMC1*^{m} with maximum sequence identities of 13.75 % and a Cryo-EM structure of calcium-bound nhT- MEM16 lipid scramblase in nanodisc (PDBs: 6QM6, 6QMA, 6QM9, and 4WIT). Additionally, the BlastP query for template search in the PDB returned no successful hits. Consequently, all the predicted structural models from Robetta and Phyre2 were evaluated in the Molprobity server.

The top-scoring models of *TMC1*$^{w+}$ and *TMC1*^{m} from Molprobity exhibited 97.27 % and 97.12 % Ramachandran-favored rotamers, respectively. Drastic structural re-adjustments were observed in *TMC1*^{m}, in contrast to *TMC1*$^{w+}$. The helices at the distal C-terminal end displayed significant deviations, leading to the closing of the inner channel. Moreover, many helical repositioning, elongations, and deletions were also witnessed.

3.5. Two coding genotypic variabilities within MET genes

WES results were re-analyzed to understand the phenotypic heterogeneity between II and 2 and II-3 affected individuals at low frequencies to understand the variation of the genotypes for genes interacting with *TMC1* protein (Supplementary Table S1). Entirely 22 variants were detected in the heterozygous state (one in *LHFPL5*, 4 in *CIB2,* and 18 in *TMC2*) within sample II-3, though they were absent in the II-2 sample. Among them, only two variants within the TMC2 gene were coding - c.368G > A (p.Arg123Lys) and c.614A > G (p.Gln205Arg).

3.6. Structure validation

The sequence determines the specific proteomic structure, while such a structure determines proteomic function. Consequently, the complete and valid structure is essential for understanding its behavior, such as binding affinities, domain, and motifs. The 3D structure of targeted proteins was validated through Molprobility to validate the chemistry for the investigated protein, including bad angles, rotamers, and amino acid patterns. All such features were refined, and the structure was prepared for docking.

3.7. Structure comparison

The structure of *TCM1* published by Ballesteros et al. (Oza et al., 2018) was compared with the predicted structure used in this study. Both models for *TCM1* were submitted to the UCLA structure validation SERVER (https://saves.mbi.ucla.edu/) for Ramachandran analysis, ERRAT, and Verify3D predictions justifying the selection of the model used in this study. The results elucidated that the Ramachandran quality of the mouse *TMC1* structure predicted by Ballesteros et al. was more significant than our predicted structure for human *TMC1.* For human TMC1 predicted in this study, 71 % of amino acids were located within the most favorable region, 18 % were found in the additional regions, and 5 % were located within allowed regions. In comparison, only 3 % of residues were located within the disallowed region, as shown in Table 2. For mouse TMC1 predicted by Ballesteros et al., 94.8 % of amino acids were located within the most favorable region, 18 % of.

the residues were located in the additional regions, and 3.9 % of residues were located within allowed regions. In comparison, only 0.7 % of residues were located within the disallowed region, as

Table 2
Structure evaluation and comparison of TMC1 human and TMC1 mouse proteins.

Model	ERRA T	Verify 3D	PDBsum Generate Ramachandran Plot										
			Residues in most favored regions [A,B,L]	%[A,B,L]	Residues in additional allowed regions [a,b,l, p]	%[a,b,l,p]	Residues in generously allowed regions [~a,~b,~l,~p]	%[~a,~b,~ l,~p]	Disallowed Residues	%Disallowed Residues	Total residues	Bad contacts / 100 residues	Overall G- factor
TMC1	80.20	40.53	490	71.70 %	129	18.90 %	39	5.70 %	25	3.70 %	760	0.8	−0.7
(human)	%	%											
TMC1	57.43	39.86	723	94.80 %	30	3.90 %	5	0.70 %	5	0.70 %	858	2.9	−0.1
(mouse)	%	%											

shown in Table 2. But ERRAT quality factor for our predicted structure (80.2 %) was more significant than the already published TMC1 structure (57.43 %) (Fig. 2B,2D). ERRAT is a so- called "overall quality factor" for nonbonded atomic interactions, with higher scores indicating higher quality. The generally accepted range is > 50 for a high-quality model (Ballesteros et al., 2018). Similarly, the Verify3D (Ballesteros et al., 2018) score for our predicted structure (40.53 %) was slightly more significant than the already published TMC1 structure (39.86 %) (Fig. 2).

3.8. TMC2-3D structural development

To obtain the complete 3D structure of *TMC2*^{WT}, *TMC2*^{R123K}, *TMC2*^{Q205R,} and *TMC2*$^{R123K+Q205R}$, multi-scale structure-based studies were carried out. The model of *TMC2*^{WT} with the value of C-scores −1.01 was selected. C-score is typically in the range of [-5, 2], where a C-score of a higher value signifies a model with higher confidence. A Ramachandran plot designated the presence of > 86 % residues of modeled structures in the sterically allowed region, while 0.16 % residues were considered outliers. Parameters such as peptide bond planarity, non-bonded interactions, Cα-tetrahedral distortion, main chain H-bond energy, and overall G-factor for the modeled structure were all lying in the favorable range. The optimized and modeled structure is illustrated in Fig. 3.

3.9. p. Arg123Lys and p. Gln205Arg led to conformational alterations in TMC2 3D structure

To explore the effect of variants on *TMC2* structure, predicted structures of *TMC2*^{R123K}, *TMC2*^{Q205R,} and *TMC2*$^{R123K+Q205R}$ were superimposed with *TMC2*^{WT} by UCSF Chimera. An RMSD value of 1.1 Å, 0.8 Å, and 0.9 Å, respectively, depict the structure's conformational changes. Through comparative analyses of *TMC2*^{R123K}, *TMC2*^{Q205R,} and *TMC2*$^{R123K+Q205R}$ with *TMC2*^{WT,} pronounced conformational alterations were witnessed. Regarding *TMC2*^{R123K}, conformational variations in Thr74-Glu85 and Arg358-Gly369 of the cytoplasmic domain resulted in the helical region's extension. A considerable conformational change was observed at the region encompassing Phe520-Ile714 residues, comprising a transmembrane helical domain and an extracellular topological domain at the c-terminus (Fig. 4).

Regarding *TMC2*^{Q205R}, the mutation from Lysine to Arginine brings alterations within the *N*-terminal cytoplasmic domain - a helix from Thr74-Gly84 that is elongated upon mutation. Substantial conformational changes were observed in the transmembrane helical and extracellular topological domains. Remarkably, upon mutation, loop region Gly638-Phe641 transformed into α-helical conformation resulting in the extension of the α-helix encompassing Ala628-Leu662 residues.

Regarding *TMC2*$^{R123K+Q205R}$, conformational variations were observed at the Lys72-Gly84 region of the cytoplasmic domain, which resulted in the extension of the α-helix. Moreover, significant conformational alterations were observed, specifically in the proximity of Ser650-Val710 and Ser802-Ser822 residues, resulting in an alteration of the active site.

3.10. R123K and Q205R variations in TMC2 disrupted binding between TMC1^{N199I} *and TMC2 proteins*

To determine the *TMC2*-specific binding regions required for interaction with *TMC1*^{N199I}, molecular docking studies were performed. By comparing the residual contributions of mutated (*TMC2*^{R123K}, *TMC2*^{Q205R,} and *TMC2*$^{R123K+Q205R}$) and *TMC2*^{WT} in *TMC1*^{N199I} binding, this study investigated the mutational effect on binding modalities. Regarding *TMC2*^{WT}/*TMC1*^{N199I} complex, Lys399, Arg454, Gln457, and Lys807 residues of *TMC2*^{WT} were

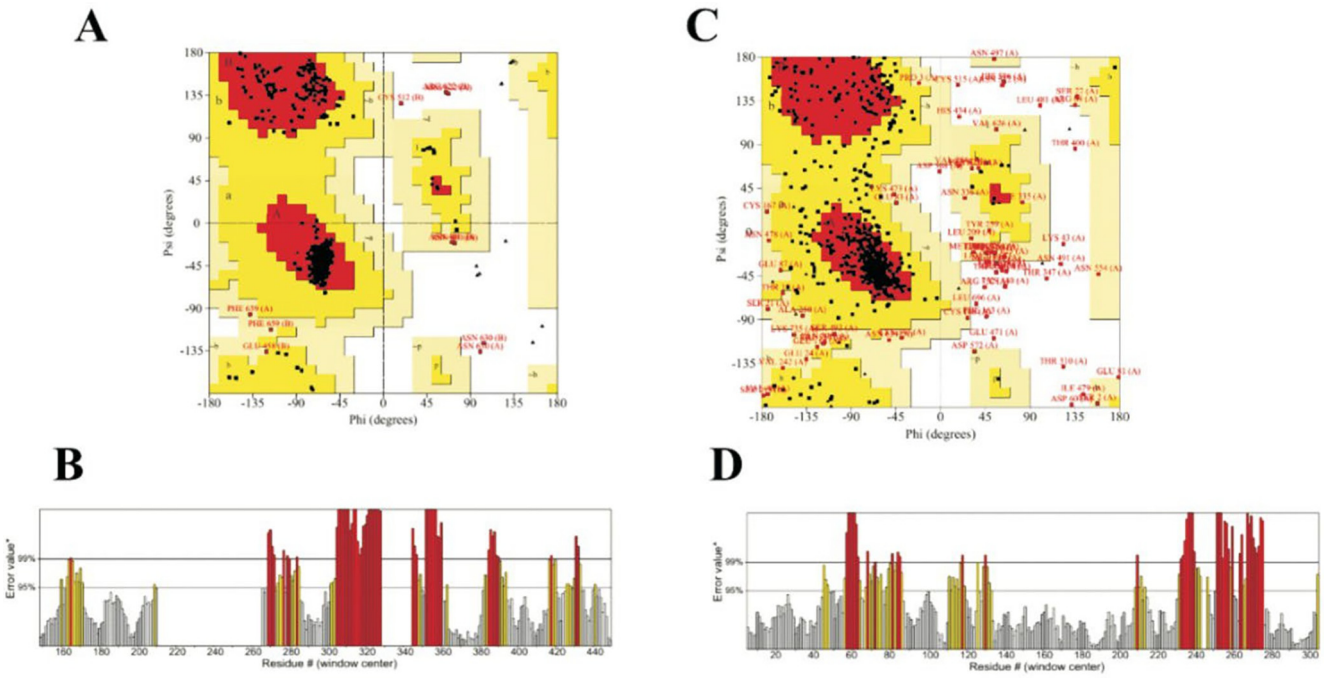

Fig. 2. Structure comparison and evaluation of human and Mouse *TMC1*. **(A)** Ramachandran values for mouse *TMC1*. **(B)** ERRAT factor for mouse *TMC1* **(C)** Ramachandran values for human *TMC1*. **(D)** ERRAT factor for human *TMC1*.

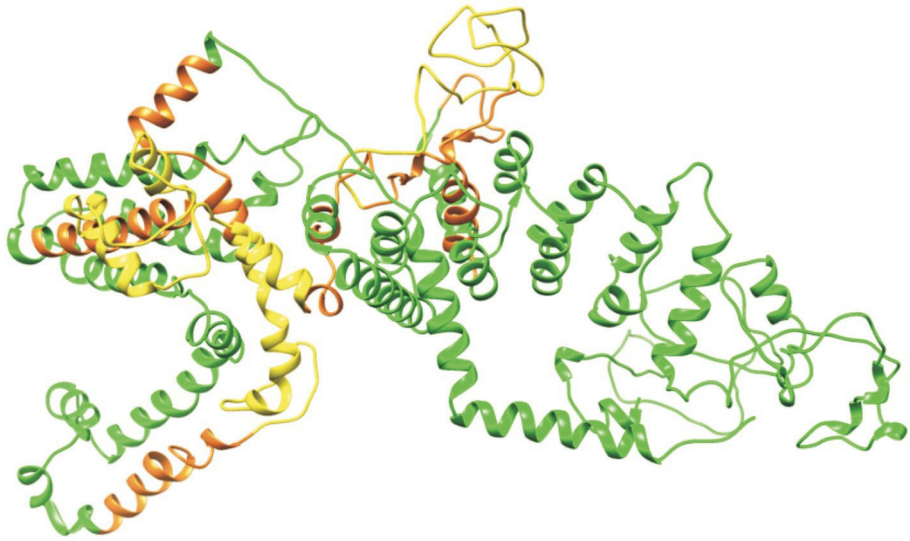

Fig. 3. 3D model of *TMC2*. TMC2 comprises three topological features: Cytoplasmic domain (green), Helical *trans*-membrane domain (orange), and extracellular domain (yellow).

hydrogen bonding with Tyr490, Val708, and Asp729 residues of $TMC1^{N199I}$ (Fig. 5A). In addition to H-bonding, several $TMC2^{WT}$ residues were involved in hydrophobic contacts, as illustrated in Table 3. The binding energy value for the complex is −21.37 kcal/-mol (Supplementary 2).

Regarding $TMC2^{123K}$/$TMC1^{N199I}$ complex, this study identified the involvement of *TMC2* specific Glu58, Met259, Val262, Asn263, and Ser305 residues being intricately involved in H-bond formation with $TMC1^{N199I}$. Asn30, Arg42, Asn634, Asp729, and Lys735 residues of $TMC1^{N199I}$ participated in developing hydrogen bonds. Upon binding of $TMC2^{123K}$ with $TMC1^{N199I}$, the binding energy of the selected complex was −15.66 kcal/mol. Interestingly, $TMC2^{123K}$ exhibited a differing binding pattern than $TMC2^{WT}$ (Fig. 5B). Overall, R123K mutation within *TMC2* disrupted the formation of an interactive surface for $TMC1^{N199I}$ binding. Due to mutations of R123k and Q205, complex of tmc2 became more stable as it distract pattern of compex.

In $TMC2^{Q205R}$/$TMC1^{N199I}$ complex, Val475, Met525, His682, Arg610 and Tyr614 residues of $TMC2^{Q205R}$ were involved in H-bonding with $TMC1^{N199I}$ (Fig. 5C). Furthermore, such hydrogen-bond contacts were strengthened by hydrophobic associations. Upon binding of $TMC2^{123K}$ with $TMC1^{N199I}$, the binding energy of

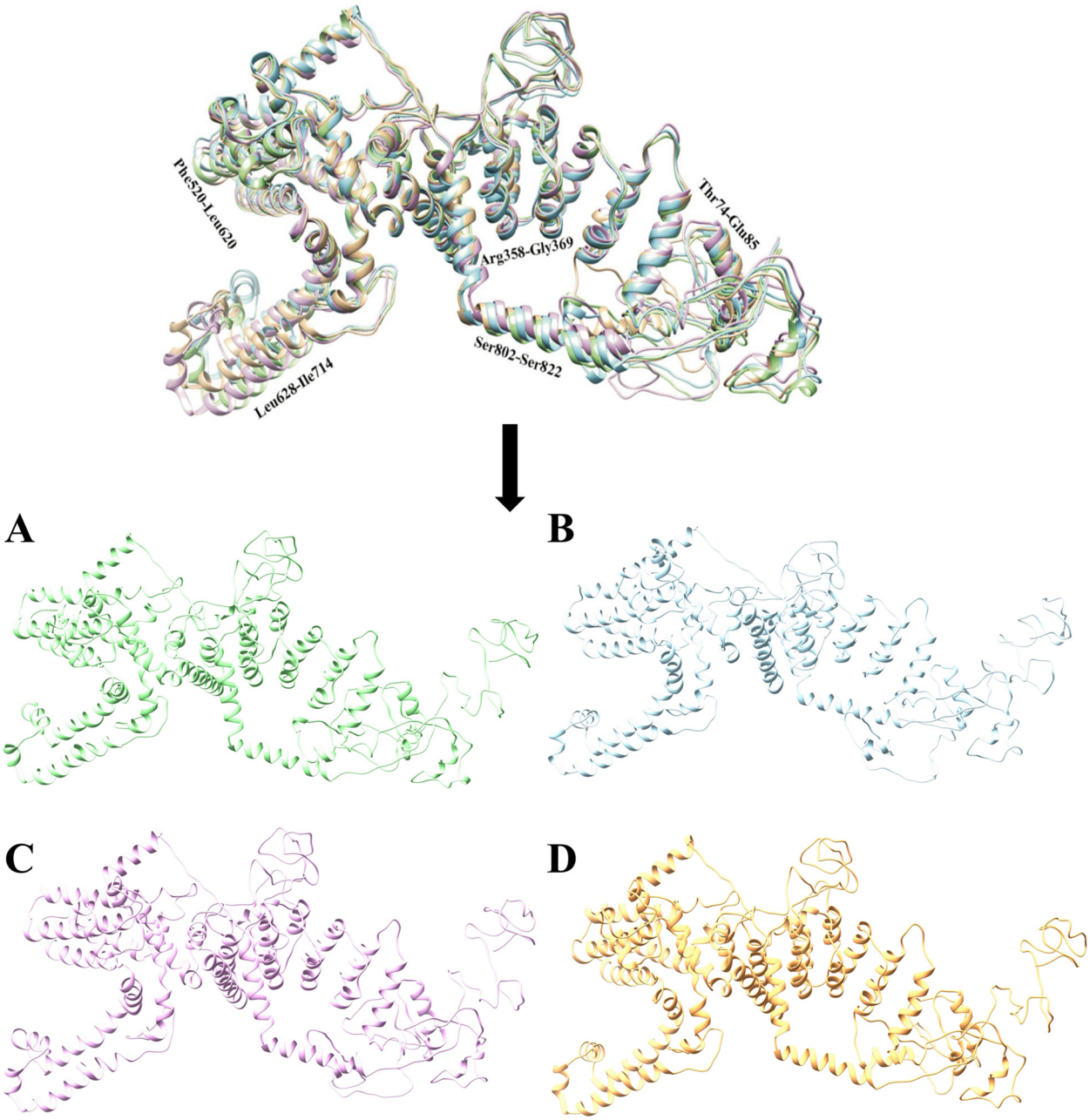

Fig. 4. Comparative analysis of *TMC2*^{WT}, *TMC2*^{R123K}, *TMC2*^{Q205R} and *TMC2*$^{R123K+Q205R}$. The above panel represents the super- imposition of ***TMC2***^{WT} (spring green color) with ***TMC2***^{R123K} (sky blue), ***TMC2***^{Q205R} (plum color), and ***TMC2***$^{R123K+Q205R}$ (tan color), while regions indicating the variation in the conformation of mutated and wild type *TMC2* are also labeled. The below panel represents the individual TMC2 structures. **(A)** *TMC2*^{WT}, **(B)** *TMC2*^{R123K}, **(C)** *TMC2*^{Q205R}, **(D)** *TMC2*$^{R123K+Q205R}$.

the selected complex was −28.50 kcal/mol. *TMC2*^{Q205R}. However, upon docking of mutated *TMC2*^{Q205R} with *TMC1*^{N199I}, it was observed that mutation has consider- able effects on the binding site of *TMC1*^{N199I}. Similar to *TMC2*^{WT}, Ser716-Gln737 residues of the extracellular topological domain revealed a significant contribution in *TMC1*^{N199I} binding (Table 3). Regarding *TMC2*$^{123K+Q205R}$-*TMC1*^{N199I} complex, this study identified the involvement of *TMC2*$^{-}$ specific Asn263, Asn551, Arg561, Arg571, and Asn776 residues involved in hydrogen bonding with Met211, Lys164, Glu171, and Leu730 of *TMC1*^{N199I} (Fig. 5D). Several residues were involved in the hydrophobic association. The binding energy value for this complex was −25.53 kcal/mol.

Mutated *TMC1*^{N199I} interacted with *TMC2* residues that were physically distant from the region, which is considered a crucial domain for interaction. These results predicted the effective binding of the *TMC1* and *TMC2* interactions, which can be further validated by computer-based simulations and experimental studies in the future to provide efficient findings.

In summary, such results demonstrated that R123K and Q205R variations in *TMC2* disrupted the binding between *TMC1*^{N199I} and the *TMC2* proteins, which can explain the severity of hearing loss (10–20 dBL) observed for II-3 at low frequencies when compared to her sister, II-2. In addition, according to the recommendations for autosomal recessive segregation evidence (PP1) listed within the American College of Medical Genetics and Genomics/Association for Molecular Pathology (ACMG/AMP) variant interpretation guidelines (McKenna et al., 2010); such a mutation scored 1.2 and therefore implying moderate recommendations. Furthermore, *TMC1* is listed as an autosomal dominant determinant of NSHL with solid supportive evidence 12.5 assigned points (out of 18)

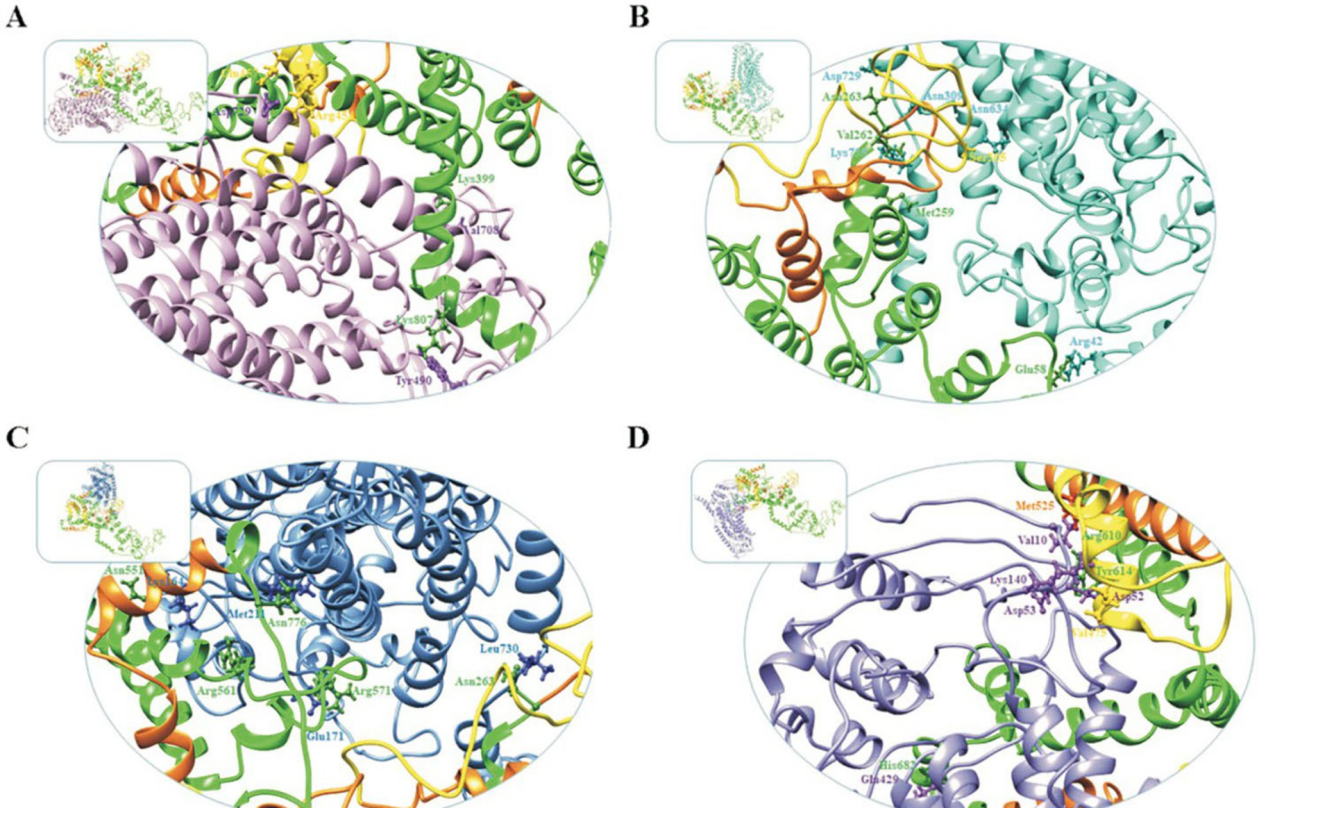

Fig. 5. Comparative binding analysis of *TMC1*^{N199I} with *TMC2*^{WT} and mutated *TMC2*^{123K}, *TMC2*$^{Q205R.}$ and *TMC2*$^{123K+Q205R}$ complexes. Optimal docked complexes of (A) *TMC2*^{WT}/*TMC1*^{N199I} *TMC2*^{123K}/*TMC1*^{N199I} (C) *TMC2*$^{R123K+Q205R}$/*TMC1*^{N199I} (D) *TMC2*^{123K}/*TMC1*^{N199I}. *TMC2* domains, including cytoplasmic, helical *trans*-membrane, and extracellular domains, are demonstrated by green, orange, and yellow colors, *TMC1* bound with *TMC2*^{R123K}, *TMC2*$^{Q205R.}$ and *TMC2*$^{R123K+Q205R}$ are illustrated in plum, sky blue, cornflower blue, and purple color, respectively. Residues involved in hydrogen bonding are represented in their respective ribbon colors and illustrated in ball-and- stick representation.

according to the ClinGen Clinical Validity Framework (11/3/2017 version – https://www.clinicalgenome.org), encompassing both case-level family segregation or supportive case-control data and also genomic experimental proof that backs up such gene-disease link. Further details can be found on the Clinical genome mutational variant curation repository (https://www.clinicalgenome.org).

Upon interaction of TMC1wt- TMC2wt, the binding energy of complex was –21 kcal/mol. TMC1 shows phe 203, Ile204, Phe207, ILE285, HIS 606, SER 657, LYS 735, MET 736, GLN 737 binding residues with TMC2. TMC2wt bind with *N*-terminus of TMC1wt. Interestingly TMC1wt-TMC2wt complex shows different binding pattern as compared to mutant structures of TMC1- TMC2 (Fig. 6).

4. Discussion

Hearing impairment is a monogenic disorder and one of the most common health problems worldwide. Reports claim that 4 % of the UAE population suffers from HL defects, estimated at 155 patients per 100,000 live births (Scott et al., 1996; Hilgert et al., 2008). This study analyzed a UAE family affected with ARNSHL, using WES followed by Sanger sequencing validation bioinformatics analysis to assess the impact of detected mutations. Results revealed a missense mutation (c.596 A > T) in exon 11, resulting in the substitution of an Arginine with Isoleucine at position 199 (p. Asn199Ile). The functional consequences of Asn199Ile mutation on human *TMC1* function were assessed using Polyphen (score = 1) and SIFT, predicting a damaging and harmful impact, respectively. Additionally, this study demonstrated Asn199 being conserved across all analyzed lineages through comparative analysis.

Previous studies identified mutations in *TMC1* that were associated with HL. Earlier studies in the Tunisian population reported three nonsense mutations in the *TMC1* gene (p.R34X, p.R389X and p.W588X) were reported in previous studies in the Tunisian population (Schrauwen et al., 2013; Lebeko et al., 2015; Bakhchane et al., 2015). A novel pathogenic homozygous mutation causing nonsyndromic hearing loss was reported to be present in *TMC1* exon 20 (c.1810C > G; p. Arg604Gly) within the Moroccan population, causing structural changes in *TMC1* protein (Lebeko et al., 2015). In Sudan, Tunisia, and Jordan, a nonsense mutation in the EC2 domain of *TMC1* exon 15, c.1165C > T p.R389X, was found (Jia et al., 2020; Sadeghian et al., 2019; Nishio and Usami, 2021). Within intron 23, the c.2260 + 2 T mutation was identified, along with another mutation in exon 7, c.100C N T (p. R34X), within the Tunisian population (Sadeghian et al., 2019). This same mutation in exon 7 of *TMC1* was also detected in a family from Algeria (Nishio and Usami, 2021). Furthermore, *TMC1* is listed as an autosomal dominant determinant of NSHL with supportive evidence 12.5 assigned points (out of 18) according to the ClinGen Clinical Validity Framework (11/3/2017 version – https://www.clinicalgenome.org). It encompasses both case-level family segregation, supportive case-control data, and experimental genomic proof that backs up such gene-disease links.

The mutational spectrum of this gene can be extended by adding a few more previously reported mutations. A novel missense mutation in exon 20 (c.1979C > T, p. P660L) was found in the conserved domain T5-T6 of *TMC1*. Additionally, the three novel mutations p. S596R, p.N199I and c.1404 + 1G > T (skipping of exon 16) were also reported (Lebeko et al., 2015; Sadeghian et al., 2019). The

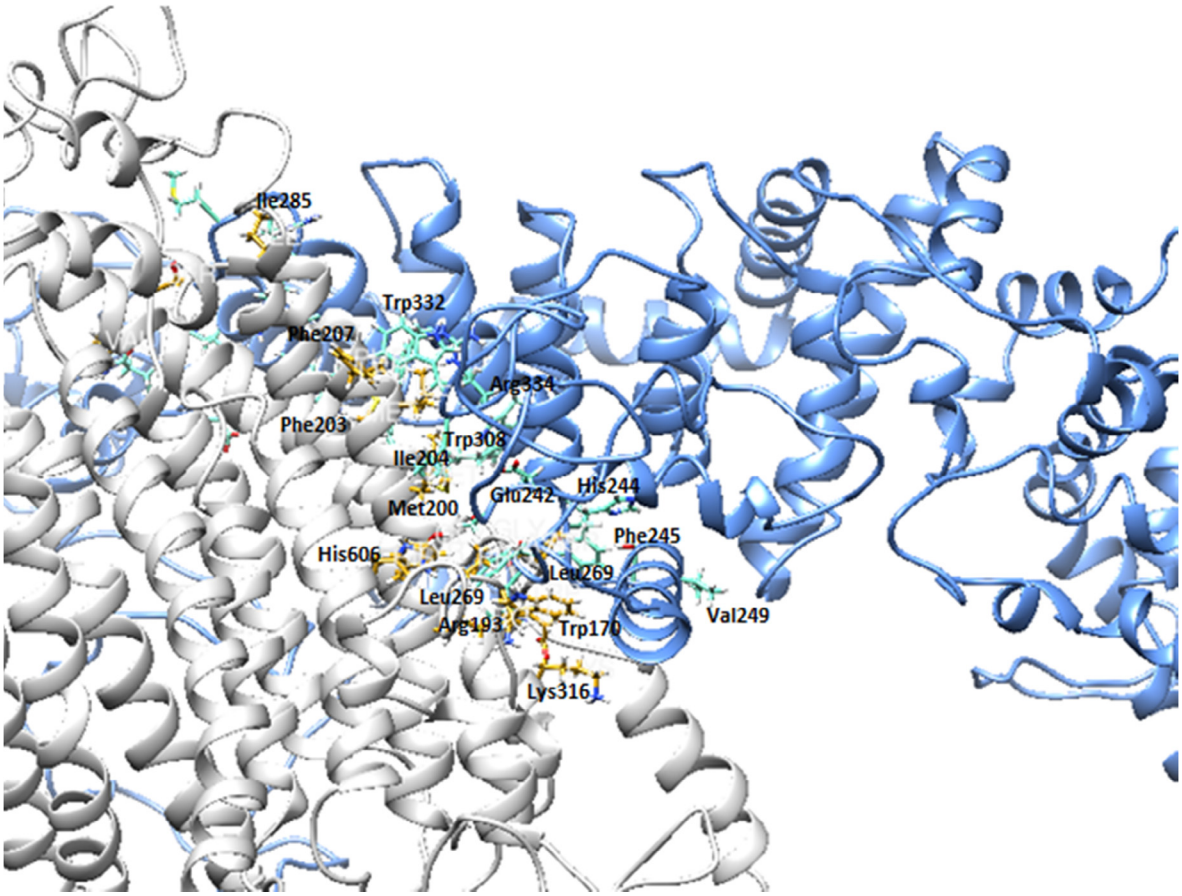

Fig. 6. Docking structure of TMC1wt-TMC2wt. TMC1wt shown in grey color while TMC2wt shown in blue. Yellow and cyan color bonds are interacting residues of TMC1wt and -TMC2wt vice versa.

mutation identified in the UAE family analyzed in this study suggests that it contributes to a minority of all ARNSHL cases in the UAE population. All such results set forth a remarkable contribution to ARNSHL by mutations in the *TMC1* gene. The identified mutations were detected in the investigated family, suggesting that they can significantly contribute to DFNB7- and DFNB11-forms of deafness in the UAE family.

The mutation introduced at amino acid position 123 with Arg > Lys disrupted the normal inter- action between *TMC1* and *TMC2* proteins. Similarly, the docking of mutated *TMC1* (N199I - mutation at amino acid position 205 with Arg > Glu), with *TMC2* normal protein (205Q) revealed significant changes at the structural level by disrupting the interaction of *TMC1* and *TMC2* with each other. Finally, the double mutated *TMC2* protein (123 k + 205R) was also substantially impacted. Following evaluations and comparative analyses of the interactions of two differing-mutated *TMC1* proteins with *TMC2* normal protein, the results demonstrate the damaging effect of these mutations at the proteomic structural level, possibly through disruption of normal interplays be- tween both proteins. The comparison between mutated and wild-type *TMC2* proteins resulted in several structural variations in α-helices and loops. In essence, mutations in *TMC2* affected the association of $TMC1^{N199I}$ with *TMC2*, resulting in phenotypic variability.

5. Conclusions

In conclusion, this study reported the association of *TMC1* missense mutation c.596 A > T (p.Asn199Ile) with ARNSHL in a UAE family, resulting in deleterious functional consequences. Additionally, protein docking results suggested the involvement of *TMC2* variants in the phenotypic variability observed in this particular family. Such proteins are highly interactive, and a single nucleotide polymorphism or missense mutation can devastate the structural properties and protein–protein interactions. Such mutations are highly deleterious and can cause significant damage to the normal interaction behaviors, ultimately causing hearing loss conditions.

Disclosure of funding

This research was funded by the University of Sharjah.

Declaration of Competing Interest

The authors declare that they have no known competing financial interests or personal relationships that could have appeared to influence the work reported in this paper.

Appendix A. Supplementary material

Supplementary data to this article can be found online at https://doi.org/10.1016/j.sjbs.2022.103520.

References

Bakhchane, A., Charoute, H., Nahili, H., Roky, R., Rouba, H., Charif, M., Lenaers, G., Barakat, A., 2015. A Novel Mutation in the *TMC*1 Gene Causes Nonsyndromic Hearing Loss in a Moroccan Family. Gene 574, 28–33. https://doi.org/10.1016/j.gene.2015.07.075.

Ballesteros, A., Fenollar-Ferrer, C., Swartz, K.J., 2018. Structural relationship between the putative hair cell mechanotransduction channel TMC1 and TMEM16 proteins. Elife 7, e38433.

Diaz-Horta, O., Duman, D., Foster, J., Sırmacı, A., Gonzalez, M., Mahdieh, N., Fotouhi, N., Bonyadi, M., Cengiz, F.B.B., Menendez, I., et al., 2012. Whole-Exome Sequencing Efficiently Detects Rare Mutations in Autosomal Recessive Nonsyndromic Hearing Loss. PLoS One 7, e50628. https://doi.org/10.1371/journal.pone.0050628.

Giese, A.P., Tang, Y.Q., Sinha, G.P., Bowl, M.R., Goldring, A.C., Parker, A., et al., 2017. CIB2 interacts with TMC1 and TMC2 and is essential for mechanotransduction in auditory hair cells. Nature communications 8 (1), 1–13.

Global Costs of Unaddressed Hearing Loss and Cost-Effectiveness of Interven- tions Available online: https://www.who.int/publications-detail-redirect/global-costs-of-unaddressed-hearing-loss-and-cost-effectiveness-of-interventions (accessed on 15 September 2021).

Gorlin, R.J., Gorlin, R.J., Toriello, H.V., Cohen, M.M., 1995. Hereditary Hearing Loss and Its Syndromes. Oxford University Press. ISBN 978-0-19-506552-7..

Hilgert, N., Alasti, F., Dieltjens, N., Pawlik, B., Wollnik, B., Uyguner, O., Delma- ghani, S., Weil, D., Petit, C., Danis, E., et al., 2008. Mutation Analysis of TMC1 Identifies Four New Mutations and Suggests an Additional Deafness Gene at Loci DFNA36 and DFNB7/11. Clin Genet 74, 223–232. https://doi.org/10.1111/j.1399-0004.2008.01053.x.

Hudspeth, A.J., 1989. How the 'Ear's Works Work. Nature 341, 397–404. https://doi.org/10.1038/341397a0.

Jain, P.K., Fukushima, K., Deshmukh, D., Ramesh, A., Thomas, E., Lalwani, A.K.K., Kumar, S., Plopis, B., Skarka, H., Srisailapathy, C.R.A., 1995. Human Recessive Neu- rosensory Nonsyndromic Hearing Impairment Locus Is Potential Homologue of Murine eafness (Dn) Locus. Hum Mol Genet 4, 2391–2394. https://doi.org/10.1093/hmg/4.12.2391.

Jia, Y., Zhao, Y., Kusakizako, T., Wang, Y., Pan, C., Zhang, Y., Nureki, O., Hat- tori, M., Yan, Z., 2020. TMC1 and TMC2 Proteins Are Pore-Forming Subunits of Mechano-sensitive Ion Channels. Neuron 105, 310-321.e3. https://doi.org/10.1016/j.neuron.2019.10.017.

Kalay, E., Karaguzel, A., Caylan, R., Heister, A., Cremers, F.P.M., Cremers, C.W.R.J., Brunner, H.G., de Brouwer, A.P.M., Kremer, H., 2005. Four Novel *TMC*1 (DFNB7/DFNB11) Mutations in Turkish Patients with Congenital Autosomal Recessive Nonsyndromic Hearing Loss. Hum Mutat 26, 591. https://doi.org/10.1002/humu.9384.

Kawashima, Y., Géléoc, G.S.G., Kurima, K., Labay, V., Lelli, A., Asai, Y., Makishima, T., Wu, D.K., Della Santina, C.C.C., Holt, J.R., et al., 2011. Mechanotransduction in Mouse Inner Ear Hair Cells Requires Transmembrane Channel-like Genes. J Clin Invest 121, 4796–4809. https://doi.org/10.1172/JCI60405.

Kitajiri, S.-I., McNamara, R., Makishima, T., Husnain, T., Zafar, A.U., Kittles, R.A., Ahmed, Z.M., Friedman, T.B., Riazuddin, S., Griffith, A.J., 2007. Identities, Frequencies, and Origins of *TMC*1 Mutations Causing DFNB7/B11 Deafness in Pakistan. Clin Genet 72, 546–550. https://doi.org/10.1111/j.1399-0004.2007.00895.x.

Kurima, K., Peters, L.M., Yang, Y., Riazuddin, S., Ahmed, Z.M., Naz, S., Arnaud, D., Drury, S., Mo, J., Makishima, T., et al., 2002. Dominant and Recessive Deafness Caused by Mutations of a Novel Gene, *TMC*1, Required for Cochlear Hair-Cell Function. Nat Genet 30, 277–284. https://doi.org/10.1038/ng842.

Langmead, B., Trapnell, C., Pop, M., Salzberg, S.L., 2009. Ultrafast and memory-efficient alignment of short DNA sequences to the human genome. Genome Biol. 10(3):R25. https://doi.org/10.1186/gb-2009-10-3-r25. Epub 2009 Mar 4. PMID: 19261174; PMCID: PMC2690996.

Lebeko, K., Bosch, J., Noubiap, J.J.N., Dandara, C., Wonkam, A., 2015. Genetics of Hearing Loss in Africans: Use of next Generation Sequencing Is the Best Way Forward. Pan Afr Med J 20, 383. https://doi.org/10.11604/pamj.2015.20.383.5230.

McKenna, A., Hanna, M., Banks, E., Sivachenko, A., Cibulskis, K., Kernytsky, A., Garimella, K., Altshuler, D., Gabriel, S., Daly, M., DePristo, M.A., 2010. The Genome Analysis Toolkit: a MapReduce framework for analyzing next-generation DNA sequencing data. Genome Res. 20 (9), 1297–1303. https://doi.org/10.1101/gr.107524.110. Epub 2010 Jul 19. PMID: 20644199; PMCID: PMC2928508.

Mehl, A.L., Thomson, V., 2002. The Colorado Newborn Hearing Screening Project, 1992–1999: On the Threshold of Effective Population-Based Universal Newborn Hear- ing Screening. Pediatrics 109, E7. https://doi.org/10.1542/peds.109.1.e7.

Nishio, S., Usami, S. 2021. Prevalence and Clinical Features of Autosomal Dominant and Recessive. TMC1-Associated Hearing Loss.

Oza, A.M., DiStefano, M.T., Hemphill, S.E., et al., 2018. Expert specification of the ACMG/AMP variant interpretation guidelines for genetic hearing loss. Human Mutation. 39, 1593–1613. https://doi.org/10.1002/humu.2363.

Pacentine, I.V., Nicolson, T., 2019. Subunits of the Mechano-Electrical Transduction Channel, *TMC*1/2b, Require Tmie to Localize in Zebrafish Sensory Hair Cells. PLoS Genet 15, e1007635.

Sadeghian, L., Tabatabaiefar, M.A., Fattahi, N., Pourreza, M.R., Tahmasebi, P., Alavi, Z., Hashemzadeh Chaleshtori, M., 2019. Next-Generation Sequencing Reveals a Novel Pathological Mutation in the *TMC*1 Gene Causing Autosomal Recessive Non-Syn- dromic Hearing Loss in an Iranian Kindred. Int J Pediatr Otorhinolaryngol 124, 99–105. https://doi.org/10.1016/j.ijporl.2019.05.023.

Schrauwen, I., Sommen, M., Corneveaux, J.J., Reiman, R.A., Hackett, N.J., Claes, C., Claes, K., Bitner-Glindzicz, M., Coucke, P., Van Camp, G., et al., 2013. A Sensitive and Specific Diagnostic Test for Hearing Loss Using a Microdroplet PCR-Based Ap- proach and next Generation Sequencing. Am J Med Genet A 161A, 145–152. https://doi.org/10.1002/ajmg.a.35737.

Scott, D.A., Carmi, R., Elbedour, K., Yosefsberg, S., Stone, E.M., Sheffield, V.C., 1996. An Autosomal Recessive Nonsyndromic-Hearing-Loss Locus Identified by DNA Pool- ing Using Two Inbred Bedouin Kindreds. Am J Hum Genet 59, 385–391.

Tlili, A., Rebeh, I.B., Aifa-Hmani, M., Dhouib, H., Moalla, J., Tlili-Chouchène, J., Said, M.B.B., Lahmar, I., Benzina, Z., Charfedine, I., et al., 2008. *TMC*1 but Not *TMC*2 Is Responsible for Autosomal Recessive Nonsyndromic Hearing Impairment in Tunisian Families. Audiol Neurootol 13, 213–218. https://doi.org/10.1159/000115430.

World Health Organization Global Health Estimates 2016: Disease Burden by Cause, Age, Sex, by Country and by Region., 2018.

Further Reading

Ben Saïd, M., Hmani-Aifa, M., Amar, I., Baig, S.M., Mustapha, M., Delmaghani, S., Tlili, A., Ghorbel, A., Ayadi, H., Van Camp, G., et al., 2010. High Frequency of the p. R34X Mutation in the *TMC*1 Gene Associated with Nonsyndromic Hearing Loss Is Due to Founder Effects, 14. Genet Test Mol Biomarkers, pp. 307–311. https://doi.org/10.1089/gtmb.2009.0174.

Colovos, C., Yeates, T.O., 1993. Verification of protein structures: patterns of nonbonded atomic interactions. Protein science 2 (9), 1511–1519.

Schmucker, C., Kapp, P., Motschall, E., Loehler, J., Meerpohl, J.J., 2019. Prevalence of Hearing Loss and Use of Hearing Aids among Children and Adolescents in Germany: A Systematic Review. BMC Public Health 19, 1277. https://doi.org/10.1186/s12889-019- 7602-7.

Sirmaci, A., Duman, D., Oztürkmen-Akay, H., Erbek, S., Incesulu, A., Oztürk- Hişmi, B., Arici, Z.S., Yüksel-Konuk, E.B., Taşir-Yilmaz, S., Tokgöz-Yilmaz, S., et al., 2009. Mutations in *TMC*1 Contribute Significantly to Nonsyndromic Autosomal Recessive Sensorineural Hearing Loss: A Report of Five Novel Mutations. Int J Pediatr Otorhino- laryngol 73, 699–705. https://doi.org/10.1016/j.ijporl.2009.01.005.

Venter, J.C., Adams, M.D., Myers, E.W., Li, P.W.W., Mural, R.J.J., Sutton, G.G., Smith, H. O., Yandell, M., Evans, C.A., Holt, R.A., et al., 2001. The Sequence of the Human Genome. Science 291, 1304–1351. https://doi.org/10.1126/science.1058040.